In Silico Pharmacology (2024) 12:85
https://doi.org/10.1007/s40203-024-00258-5

ORIGINAL RESEARCH

Marine natural compounds as potential CBP bromodomain inhibitors for treating cancer: an in-silico approach using molecular docking, ADMET, molecular dynamics simulations and MM-PBSA binding free energy calculations

Md. Liakot Ali[1] · Fabiha Noushin[1] · Eva Azme[1] · Md. Mahmudul Hasan[1] · Neamul Hoque[1] · Afroz Fathema Metu[1]

Received: 7 February 2024 / Accepted: 8 September 2024

Abstract

The cAMP-responsive element binding protein (CREB) binding protein (CBP), a bromodomain-containing protein, engages with multiple transcription factors and enhances the activation of many genes. CBP bromodomain acts as an epigenetic reader and plays an important role in the CBP-chromatin interaction which makes it an important drug target for treating many diseases. Though inhibiting CBP bromodomain was reported to have great potential in cancer therapeutics, approved CBP bromodomain inhibitor is yet to come. We utilized various in silico approaches like molecular docking, ADMET, molecular dynamics (MD) simulations, MM-PBSA calculations, and in silico PASS predictions to identify potential CBP bromodomain inhibitors from marine natural compounds as they have been identified as having distinctive chemical structures and greater anticancer activities. To develop a marine natural compound library for this investigation, Lipinski's rule of five was used. Sequential investigations utilizing molecular docking, ADMET studies, 100 ns MD simulations, and MM-PBSA calculations revealed that three marine compounds—ascididemin, neoamphimedine, and stelletin A—demonstrated superior binding affinity compared to the standard inhibitor, 69 A. These compounds also exhibited suitable drug-like properties, a favorable safety profile, and formed stable protein-ligand complexes. The in-silico PASS tool predicted that these compounds have significant potential for anticancer activity. Among them, ascididemin demonstrated the highest binding affinity in both molecular docking and MM-PBSA calculations, as well as a better stability profile in MD simulations. Hence, ascididemin can be a potential inhibitor of CBP bromodomain. However, in vitro and in vivo validation is required for further confirmation of these findings.

✉ Md. Liakot Ali
liakotpranto@gmail.com

[1] Department of Pharmacy, Faculty of Biological Science, University of Chittagong, Chittagong 4331, Bangladesh

Published online: 18 September 2024

Graphical abstract

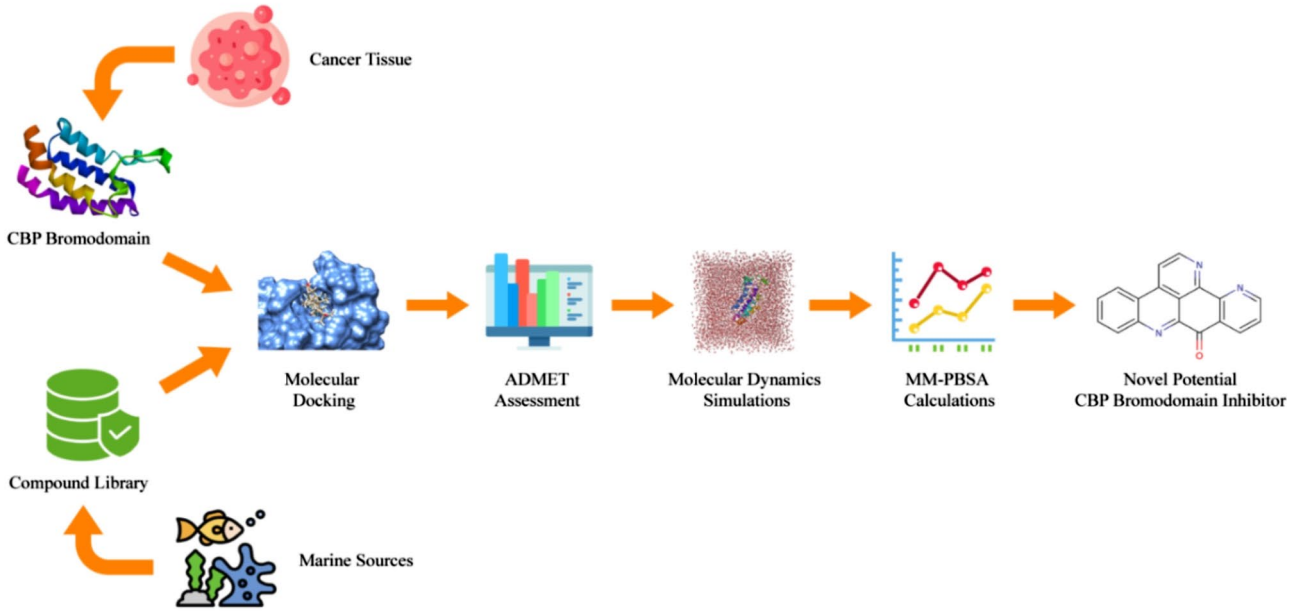

Keywords CBP · Bromodomain · Marine compound · Anti-cancer · In silico · MD simulations

Introduction

cAMP response element-binding protein (CREB) binding protein (CREBBP or CBP) is one of the important regulators of transcription that is responsible for the activation of various transcription factors in cells (Chekler et al. 2015). CBP regulates the expression of genes that govern vital cellular functions like proliferation and homeostasis and is reported to be involved in many human diseases, especially cancer (Dancy and Cole 2015). Several cancer types have shown overexpression of the CBP, which has been correlated with aggressiveness (Spiliotopoulos et al. 2017). Prostate cancer, colorectal carcinoma, acute myeloid leukemia, and large B cell lymphoma are among the diseases directly linked to CBP dysregulation (Spriano et al. 2018; Xu et al. 2022). CBP is a multidomain protein comprises of a histone acetyltransferase (HAT) domain, a CREB binding domain, a plant homology domain (PHD), various zinc finger domains as well as an epigenetic reader bromodomain (BRD) (Mujtaba et al. 2004). In addition to binding to acetylated histones during post-translational modifications of proteins, a study by Das et al. also revealed that CBP BRD is essential for promoting CBP to acetylate free histones (Das et al. 2014). As the CBP BRD is involved in multiple major biological phenomena, including DNA replication and repair, regulation of cell cycle, cellular growth as well as genomic stability, it offers a particularly intriguing new therapeutic approach in oncology. Moreover, it has been discovered to modify numerous transcription factors related to cancer, including p53, c-MYC as well as c-MYB (Mitra and Dash 2018). The experiments demonstrated that the BRD within CBP exhibits superior drug-target potential compared to its other domains (Vidler et al. 2012). Inhibiting CBP BRD with small molecules enhances conventional chemotherapy by regulating the expression of challenging oncogenic transcription factors (Dash et al. 2018). Moreover, small molecule CBP BRD inhibitors have demonstrated the capacity to hinder the differentiation of regulatory T cells (Ghosh et al. 2016). This potential application of CBP BRD inhibitors could be explored further for cancer immunotherapy. Thus, the exploration of CBP BRD inhibitors holds great promise for future cancer therapeutic advancements. Up to now, several potent small molecule CBP BRD inhibitors against cancer have been reported (Chekler et al. 2015; Conery et al. 2016; van Gils et al. 2021; Picaud et al. 2015; Rooney et al. 2014; Spiliotopoulos et al. 2017; Spriano et al. 2018; Unzue et al. 2016; Xu et al. 2022) and only two of them such as CCS1477 for hematological malignancies (phase 1/2a) (Knurowski et al. 2019) and FT-7051 for prostate cancer (phase 1) (Armstrong et al. 2021) are subjected to face the clinical trial. Therefore, further investigation is required to discover CBP BRD inhibitors that offer improved effectiveness as well as safety for clinical application against cancer.

Marine organisms are the most prevalent source of natural products with potent pharmacological activities, as the

varied structures obtained from them demonstrate the diversity of marine flora and fauna (Jiménez 2018). Because of the harsh and competitive environment found in the sea, marine organisms produce compounds with unique structural scaffolds. Many marine natural products have been found to have the potential to treat cancer thus far (Song et al. 2018). Additionally, research has shown that marine compounds have a far higher rate of anti-tumor activity than terrestrial compounds (Mayer et al. 2010). At present, the Food and Drug Administration (FDA) has approved four marine-derived pharmaceuticals for the treatment of cancer and those are brentuximab vedotin, cytarabine, eribulin mesylate, and trabectedin (Saeed et al. 2021). Yet little is known about how natural compounds derived from marine environments affect bromodomains let alone CBP BRD.

Computer-aided drug discovery (CADD) has recently gained popularity due to its ability to lower labor, consumption of time, and costs. CADD can be used to screen a large number of molecules against a particular drug target and assess their toxicity in order to identify potential bioactive compounds (Lokhande et al. 2021; Macalino et al. 2015). Following these computational techniques, the compounds will be tested experimentally to verify their activity. Thus, it lessens the need for research on a wide range of chemicals by eliminating dangerous and ineffective compounds from consideration (Pandey et al. 2021; Shaker et al. 2021). Considering this, the objective of this research was to investigate the potential of marine natural compounds as a possible inhibitor of the CBP BRD to identify effective anti-cancer agents using computer-assisted drug design techniques like molecular docking, ADMET studies, molecular dynamic simulations, the binding free energy calculation through the molecular mechanics-Poisson-Boltzmann surface area (MM-PBSA) method as well as in silico PASS prediction of anticancer activities.

Material and method

Construction of marine-derived natural compound library

Through extensive searching of previously published literature, a primary list of natural small molecules from marine sources that showed potent anti-cancer activities in vitro or in vivo was constructed (Ali et al. 2024a, 2024b; Barreca et al. 2020; Khalifa et al. 2019; Veríssimo et al. 2021). Compounds from that list were screened by Lipinski rule of five using SwissADME (Daina et al. 2017) to evaluate their drug-likeness properties to generate the final database. The final database contains a total of 114 marine-derived natural compounds (Table S1 in supplementary file).

Ligand preparation

The compounds that were included in the final database were obtained from the PubChem Database in 3D SDF format. Compounds whose 3D conformer is not present in the PubChem Database were downloaded in 2D SDF format and then converted into 3D SDF format using Open Babel software (O'Boyle et al. 2011). Prior to performing molecular docking analysis, the ligand's energy was minimized using mmff94 force field by PyRx software (Dallakyan and Olson 2015; Eberhardt et al. 2021).

Protein preparation

The Protein Data Bank was accessed to obtain the three-dimensional crystal structure of human CBP's bromodomain with an inhibitor named benzodiazepinone G02778174 (69 A) (PDB ID: 5I86; Resolution: 1.05 Å) in pdb format. The reasons for selecting this protein structure are as follows: (i) the protein originates from Homo sapiens, (ii) the structure is free of any mutations, (iii) it has a good resolution of 1.05 Å, and (iv) it contains a standard inhibitor at the active site, which is used to identify the active site for our investigation and to compare the results obtained. Next, using the Discovery Studio 2020 client software (Studio 2008), the preparation of protein structure was done by eliminating all heteroatoms as well as water molecules. Utilizing the Swiss-PDB Viewer package (Guex and Peitsch 1997), key elements such as incorrect bond order, side-chain geometry, and missing hydrogen bonds were optimized in order to produce a clean protein structure(Lokhande et al. 2022). The GROMOS96 43B1 force field (Scott et al. 1999) was employed for this procedure.

Molecular docking

Molecular docking is regarded as one of the most effective computational techniques for highlighting the bonding modes of ligands with their targets, due to its capacity to anticipate the conformation and mode of ligand binding to the receptor binding site (Chtita et al. 2022; More-Adate et al. 2024). Molecular docking was done using PyRx software (Dallakyan and Olson 2015) with a built-in docking tool named AutodockVina which uses the Broyden–Fletcher–Goldfarb–Shanno algorithm (Trott and Olson 2010). This tool utilizes genetic algorithms as well as empirical scoring functions to effectively forecast bioactive lead compound from extensive collections of compounds (Daoui et al. 2023). The co-crystalized ligand (69 A) was redocked into the binding pocket of the CBP BRD for molecular docking validation. The co-crystalized ligand was superimposed with the best pose of the re-docked co-crystalized ligand.

After that, the Root Mean Square Deviation (RMSD) was computed. The RMSD should be less than 2 Å (Acharya et al. 2019). 3D structure of protein and all ligands were imported in PyRx software and converted to pdbqt format. Co-crystalized ligand 69 A, a known inhibitor, was also added to the compound library as a reference molecule. The center of the three-dimensional grid box was set to X = − 54.18, Y = 1.90, and Z = − 10.33, and the dimensions of the grid box were (25 × 25 × 25) Å. The docking results of the compounds were calculated as well as ranked based on their highest negative values, which represented the highest binding affinities. A set of nine distinct bound conformations for each ligand, determined by their binding affinity. Only the conformational states with the lowest binding energy for the ligand molecules were selected for further investigations. The Discovery Studio 2020 program was utilized to visualize and investigate molecular properties of protein-ligand complexes such as hydrogen bonds, hydrophobic interactions as well as their bond lengths and to generate 3D and 2D figures of protein-ligand interactions.

In silico ADMET prediction

In silico ADMET (absorption, distribution, metabolism, excretion, and toxicity) analysis is an important approach to predict various drug properties which both time and money (Van De Waterbeemd and Gifford 2003). The ADMET of the selected compounds were calculated utilizing SwissADME (Daina et al. 2017), as well as ProTox-II servers (Banerjee et al. 2018). To do this, SMILES of each selected compound were collected from PubChem and uploaded onto the respective server. The compounds' pharmacokinetic and pharmacodynamic characteristics pertaining to their toxicity, excretion, distribution, metabolism, and absorption were assessed.

Molecular dynamics simulation

Molecular dynamics (MD) simulations were employed to assess the structural stability of the protein-ligand system under various conditions (Shukla and Tripathi 2020). From the molecular docking study, the top five compounds along with standard inhibitor, 69 A were chosen. These compounds underwent MD simulation using GROMACS v.2020 package (Abraham et al. 2015). In order to compare the degree of protein stability with the resulting top-docked protein-ligand complexes, an MD simulation of the apo protein was also performed. Protein and ligand topology files were generated using the CHARMM 27 force field (Bjelkmar et al. 2010), and the SwissParam server (Bugnon et al. 2023) respectively. The protein was solvated using the TIP3P water model using a triclinic box that had a minimum distance of 1 nm from the box edge. Two Na + ions were added to neutralize each system, which had the same total charge, at a concentration of 150 mM. Then, the steepest descent algorithm was used to minimize it over a period of 50,000 steps. Following that, two-step equilibrations were performed: NVT at 300 K and NPT at 1 bar. The resulting system was then used to run 100 ns of each MD simulation. The simulated trajectory was examined for structural stability using various GROMACS modules, including root mean square deviation (RMSD), root mean square fluctuation (RMSF), number of hydrogen bond formation, solvent accessible surface area (SASA), and radius of gyration (Rg).

Moreover, principal Component Analysis (PCA) was executed through Gromacs utilizing the *gmx covar* and *gmx anaeig* tools. The generation of the covariance matrix for both the apo protein and each complex involved the use of the *gmx covar* tool. This tool produces diagonal eigenvectors that depict the correlated movements within the protein. The associated eigenvalues indicate the magnitude of each eigenvector, providing insights into the atomic contributions to the motion of the protein-ligand complex system. For visualization, two-dimensional (2D) projections of the trajectory were crafted by overlaying the initial two principal components using the *gmx anaeig* tool (Kar et al. 2023).

The *gmx sham* package was utilized to calculate the 2D depiction of the free energy landscapes (FEL). This involved employing the first two eigenvectors obtained from PCA to examine the protein's conformational changes both before and after the binding of the ligand (Singh et al. 2023).

Cluster analysis

Using the *gmx cluster* tools within Gromacs, geometric clustering was carried out to investigate the variability in the protein structure post-MD simulation. The clustering algorithm by Daura et al., known as Gromos, was utilized for this purpose (Daura et al. 1999). In this analysis, a Cα RMSD cutoff of 0.15 nm was established to identify structurally similar clusters. The resulting clusters of the apo protein and each protein-ligand complex were examined to gain insights into the conformational changes in protein dynamics pre- and post-ligand binding.

Binding free energy calculation using MM-PBSA method

Following MD simulations, the binding free energy and stability of the protein-ligand complex are typically predicted using the MM-PBSA method. Additionally, it quantifies the roles that residues play in interactions between ligands and proteins. The g_mmpbsa tool, which aids in calculating the Gibbs free energy of binding (ΔG_{bind}), was utilized for this

purpose (Kumari et al. 2014a). For the ΔG_{bind} computation, the last 10 ns of the MD simulation trajectory was taken into account. ΔG_{bind} was calculated using Eq. (1).

$$\Delta G_{bind} = G_{complex} - (G_{protein} + G_{ligand}) \quad (1)$$

The total free energy of the protein-ligand complex is represented by the $G_{complex}$ in this instance. $G_{protein}$ and G_{ligand}, respectively, are the individual binding energies of the protein and ligand in the solvent. Moreover, Eq. (2) is used to calculate the individual binding energy of each component, such as protein (G), ligand (G), or protein-ligand complex (G).

$$G = E_{MM} + G_{solvation} + TS \quad (2)$$

The average molecular mechanics (MM) potential energy in a vacuum is described by the E_{MM}. $G_{solvation}$ is a notation for the free energy of solvation. The symbols T and S stand for temperature and entropy, respectively. E_{MM} and $G_{solvation}$ are calculated using Eqs. (3) and (4) respectively.

$$E_{MM} = E_{bonded} + E_{nonbonded} \quad (3)$$

$$G_{solvation} = G_{polar} + G_{nonpolar} \quad (4)$$

The bonded interaction, including bond length, bond angle, and dihedral angle, is represented by the term Ebonded. Conversely, the Enonbonded model elucidates nonbonding interactions, such as the van der Waals and electrostatic interactions. The Gpolar and Gnonpolar, respectively, represent the electrostatic and non-electrostatic contributions to the solvation free energy.

Determination of PASS prediction

The PASS program, which forecasts a compound's spectrum of activity as probable activity (Pa) and probable inactivity (Pi) was determined through the structure-activity relationship (SAR) analysis of a training set comprising over 205,000 compounds. This information was utilized to assess the anticancer activity of the selected compounds. (Lagunin et al. 2000). The range of the Pa and Pi values is 0 to 1. It is considered that the compound exhibits experimental activity if Pa > Pi. A Pa value of more than 0.7 indicates strong pharmacological potentiality, and values following $0.5 < Pa < 0.7$ show medium pharmacological activity in experiments (Lokhande et al. 2021).

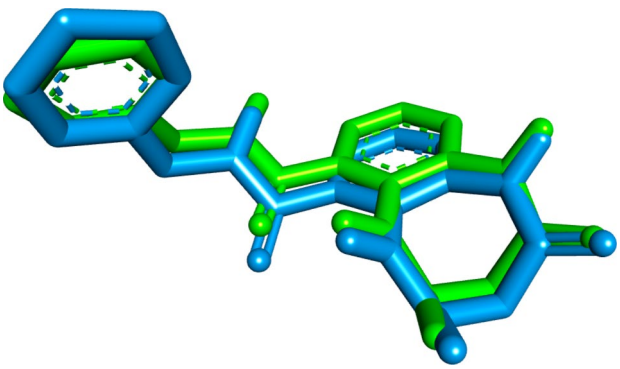

Fig. 1 Superimposition of co-crystallized ligand before (green) and after (blue) docking (RMSD = 0.625 Å)

Results and discussion

Validation of docking procedure

To validate the docking procedure, the pose with the lowest energy of the co-crystallized ligand (69 A), as generated by Autodock Vina, was compared to an experimental binding mode determined through X-ray crystallography. The docked pose and the experimental binding pose have an RMSD of 0.96 Å, which is less than 2 Å and indicates the high reliability of the docking procedure (Acharya et al. 2019). The similarity in their conformations can be observed by superimposing the two poses shown in Fig. 1.

Molecular docking

Molecular docking analysis was used to determine the best candidate on the basis of binding energy among 114 marine natural compounds. All compounds along with the reference molecule were docked into the binding site of CBP BRD. Based on the literature review, it was found that to become a potent inhibitor of CBP BRD, a molecule should interact with the specific amino acid residues of binding pocket named Pro-1110, Leu-1120, Ile-1122, Tyr-1125, Asn-1168, and Val-1174 (Dash et al. 2018).

According to molecular docking, ten compounds, listed in Table 1 showed greater affinities for binding to the receptor than the reference ligand 69 A which had a binding energy of − 8.8 kcal/mol to the CBP BRD. With an equal binding energy of − 10.1 kcal/mol, stelletin A and ascididemin from our natural marine compound library displayed the highest binding affinity to the receptor. Moreover, neoamphimedine, amphimedine, and deoxytopsentin, along with the first two ligands, showed notable binding affinities, having binding energies of − 10 kcal/mol, − 9.4 kcal/mol and − 9.4 kcal/mol, respectively, when compared to the reference ligand 69 A. Consequently, we have targeted the top five ligands—stelletin A, ascididemin, neoamphimedine, amphimedine, and deoxytopsentin—for further investigation.

Table 1 List of the top screened compounds with their PubChem ID, binding affinities with CBP BRD, and marine sources

SN	Compound	PubChem ID	Binding energy (kcal/mol)	Marine source
1	Stelletin A	5,352,083	− 10.1	*Jaspis stellifera* (Ebada et al. 2010)
2	Ascididemin	189,219	− 10.1	*Cystodytes dellechiajei* (Dassonneville et al. 2000)
3	Neoamphimedine	10,041,259	− 10	*Xestospongia carbonaria* (De Guzman et al. 1999)
4	Amphimedine	100,819	− 9.4	*Xestospongia sp.* (De Guzman et al. 1999)
5	Deoxytopsentin	183,527	− 9.4	*Topsentia genitrix* (Pon Sathieshkumar and Nagarajan 2017)
6	Deoxyamphimedine	9,994,837	− 9.3	*Xestospongia sp* (Tasdemir et al. 2001)
7	Bromotopsentin	183,528	− 9.2	*Topsentia genitrix* (Gupta et al. 2007)
8	Stellettin A	6,440,683	− 9.2	*Stelletta tenuis* (Su et al. 1994)
9	Bromodeoxytopsentin	400,452	− 9.1	*Spongosorites sp.* (Oh et al. 2006)
10	Rhabdastrellic Acid-A	21,582,592	− 9	Rhabdastrella globostellata (Li et al. 2010)
	Reference Molecule (69 A)		− 8.8	

The protein-ligand interaction analysis of the top five compounds and reference molecule was summarized in Table 2; Fig. 2. Now, docking simulation showed that reference molecule (69 A) stabilized its protein-ligand complex by forming two hydrogen bonds with Asn-1168 and nine hydrophobic interactions with seven different amino acid residues of CBP BRD such as Leu-1120, Pro-110, Arg-1173, Val-1115, Val-1174, Phe-1111 as well as Ile-1122 (Fig. 2; Table 2).

Stelletin A (IUPAC name: (3E,3aS,5aR,9aR,9bS)-3a,6,6,9a-tetramethyl-3-[(3E,5E)-6-(5-methyl-6-oxopyran-2-yl)hepta-3,5-dien-2-ylidene]-4,5,5a,8,9,9b-hexahydro-1 H-cyclopenta[a] naphthalene-2,7-dione), one of the top compounds with a fused decahydrocyclopenta[a]naphthalene core and multiple side chains, was found through docking analysis to interact with the protein primarily via its oxo-pyran group. This compound was observed to form two hydrogen bonds as well as fourteen hydrophobic interactions with the CBP BRD (Fig. 2 and Table 2). This molecule formed two conventional hydrogen bonds, one with Arg-1169 and another with Arg-1173, and also engaged in a pi-pi t-shaped hydrophobic interaction with Tyr-1125. Apart from these three interactions, stelletin A also showed two alkyl interactions with Leu-1120 and Val-1174 which also formed one pi-alkyl bond with the compound. Moreover, Pro-1110, Ile-1122, and Met-1160 formed three hydrophobic alkyl interactions. Stelletin A also formed two hydrophobic bonds with Ala-1164, one is alkyl type and another one is pi-alkyl in nature. In addition to this, this compound also formed three pi-alkyl interactions with Phe-1111, Val-1115 as well as Tyr-1167.

Another top compound, ascididemin (IUPAC name: 2,12,15-triazapentacyclo[11.7.1.03,8.09,21.014,19]henicosa-1,3,5,7,9(21),10,12,14(19),15,17-decaen-20-one) has the same binding affinity as stelletin A (− 10.1 kcal/mol). It is a complex polycyclic compound classified as a pyridoacridine alkaloid. The core structure of ascididemin is a fused tricyclic system consisting of a quinoline and a phenanthridine ring. Docking analysis revealed that the π-cloud of several aromatic rings in the compounds played a role in forming pi-alkyl interactions with the protein, while multiple -NH groups were responsible for establishing hydrogen bonds. It formed four hydrogen bonds as well as fourteen hydrophobic interactions with the protein (Fig. 2 and Table 2). Interestingly, all hydrophobic interactions formed by this compound were pi-alkyl in nature. Ascididemin stabilized its protein-ligand complex by forming two conventional hydrogen bonds with Asn-1168 and another two hydrogen bonds and one pi-alkyl bond with Pro-1110. Moreover, this compound also formed four pi-alkyl bonds with Val-1174 as well as three p-alkyl bonds with Val-1115 and Leu-1120 each. Furthermore, it established two pi-alkyl interactions with Ile-1122 and one pi-alkyl interaction with Ala-1164.

Neoamphimedine (IUPAC name: 10-Methyl-8 H-benzo[b]pyrido[4,3,2-de][1,8]phenanthroline-8,9(10 H)-dione) is a pyridoacridine alkaloid which demonstrated a binding energy of – 10 kcal/mol. The compound features a fused tricyclic system similar to ascididemin, comprising a quinoline and a phenanthridine ring, with an additional fused benzene ring, making it a tetracyclic structure. Its interaction with the protein was primarily driven by multiple -NH and carbonyl groups that formed hydrogen bonds, as well as the π-cloud of multiple aromatic rings that contributed to pi-alkyl interactions. It established two conventional hydrogen bonds with Asn-1168 and one with Pro-1110. Pro-1110 was also involved in forming a carbon-hydrogen bond. Additionally, Neoamphimedine formed two carbon-hydrogen bonds with Met-1133 and Ala-1164. It also formed one alkyl bond each with Val-1115, Met-1160,

Table 2 Docking based molecular interactions of top five marine natural compounds and reference molecule 69 A with CBP BRD

Compounds	Binding energy (kcal/mol)	Interacting amino acid	Bond type	Bond distance
Stelletin A	− 10.1	Arg-1169	Conventional hydrogen Bond	2.19
		Arg-1173	Conventional hydrogen Bond	2.59
		Tyr-1125	Pi-Pi T-shaped	5.47
		Val-1174	Alkyl	4.82
			Alkyl	4.39
			Pi-Alkyl	4.69
		Leu-1120	Alkyl	4.39
			Alkyl	4.39
		Pro-1110	Alkyl	5.36
		Ile-1122	Alkyl	4.62
		Met-1160	Alkyl	5.23
		Ala-1164	Alkyl	3.93
			Pi-Alkyl	4.68
		Val-1115	Pi-Alkyl	4.62
		Phe-1111	Pi-Alkyl	5.01
		Tyr-1167	Pi-Alkyl	5.33
Ascididemin	− 10.1	Asn-1168	Conventional Hydrogen Bond	2.41
			Conventional Hydrogen Bond	1.93
		Pro-1110	Conventional Hydrogen Bond	1.93
			Conventional Hydrogen Bond	1.87
		Leu-1120	Pi-Alkyl	5.15
			Pi-Alkyl	4.45
			Pi-Alkyl	5.32
		Ile-1122	Pi-Alkyl	4.99
			Pi-Alkyl	4.38
		Val-1174	Pi-Alkyl	4.33
			Pi-Alkyl	4.53
			Pi-Alkyl	5.18
			Pi-Alkyl	4.10
		Pro-1110	Pi-Alkyl	5.13
		Val-1115	Pi-Alkyl	5.38
			Pi-Alkyl	4.47
			Pi-Alkyl	4.67
		Ala-1164	Pi-Alkyl	4.95
Neoamphimedine	− 10	Asn-1168	Conventional Hydrogen Bond	2.52
			Conventional Hydrogen Bond	2.12
		Pro-1110	Conventional Hydrogen Bond	2.73
			Carbon Hydrogen Bond	3.05
		Met-1133	Carbon Hydrogen Bond	2.86
		Ala-1164	Carbon Hydrogen Bond	2.79
			Alkyl	4.39
		Met-1160	Alkyl	5.17
		Val-1115	Alkyl	5.44
		Pro-1110	Pi-Alkyl	5.42
			Pi-Alkyl	5.32
		Leu-1120	Pi-Alkyl	4.41
			Pi-Alkyl	5.30
			Pi-Alkyl	4.02
		Val-1174	Pi-Alkyl	4.34
			Pi-Alkyl	4.76
			Pi-Alkyl	3.97
			Pi-Alkyl	4.59
		Val-1115	Pi-Alkyl	4.48
			Pi-Alkyl	5.01
		Ala-1164	Pi-Alkyl	5.08

Table 2 (continued)

Compounds	Binding energy (kcal/mol)	Interacting amino acid	Bond type	Bond distance
		Ile-1122	Pi-Alkyl	4.69
		Phe-1111	Pi-Alkyl	4.97
Amphimedine	− 9.4	Asn-1164	Conventional Hydrogen Bond	2.05
		Phe-1111	Carbon Hydrogen Bond	2.45
		Tyr-1125	Carbon Hydrogen Bond	2.95
			Carbon Hydrogen Bond	3.02
		Met-1133	Carbon Hydrogen Bond	2.87
		Met-1160	Carbon Hydrogen Bond	3.00
			Alkyl	5.33
		Ala-1164	Alkyl	4.43
		Val-1115	Alkyl	5.39
		Phe-1111	Pi-Alkyl	5.31
		Pro-1110	Pi-Alkyl	5.23
			Pi-Alkyl	5.12
		Leu-1120	Pi-Alkyl	4.42
			Pi-Alkyl	5.27
			Pi-Alkyl	4.00
		Val-1174	Pi-Alkyl	4.38
			Pi-Alkyl	4.96
			Pi-Alkyl	4.40
			Pi-Alkyl	4.00
		Val-1115	Pi-Alkyl	4.36
			Pi-Alkyl	4.88
		Ala-1164	Pi-Alkyl	5.11
		Ile-1122	Pi-Alkyl	4.88
Deoxytopsentin	− 9.4	Pro-1114	Conventional Hydrogen Bond	2.00
		Asn-1168	Conventional Hydrogen Bond	2.72
		Pro-1110	Conventional Hydrogen Bond	2.67
			Carbon Hydrogen Bond	2.09
		Val-1174	Pi-Sigma	2.68
		Pro-1110	Pi-Alkyl	4.67
		Leu-1120	Pi-Alkyl	4.12
			Pi-Alkyl	4.28
			Pi-Alkyl	5.21
		Val-1174	Pi-Alkyl	5.20
			Pi-Alkyl	4.55
		Leu-1119	Pi-Alkyl	5.21
		Val-1115	Pi-Alkyl	5.03
			Pi-Alkyl	4.75
		Ala-1164	Pi-Alkyl	4.60
Reference Molecule (69 A)	− 8.8	Asn-1168	Conventional Hydrogen Bond	1.83
			Conventional Hydrogen Bond	1.94
		Leu-1120	Pi-Sigma	3.98
		Pro-1110	Alkyl	3.73
			Alkyl	5.47
		Arg-1173	Alkyl	5.22
		Val-1115	Alkyl	4.77
		Val-1174	Alkyl	4.36
			Pi-Alky	5.11
		Phe-1111	Pi-Alky	4.76
		Ile-1122	Pi-Alky	4.77

and Ala-1164. Moreover, the compound exhibited four, three, two, and two pi-alkyl hydrophobic interactions with Val-1174, Leu-1120, Val-1115, and Pro-1110, respectively. Furthermore, it formed one pi-alkyl hydrophobic interaction each with Ile-1122, Ala-1164, and Phe-1111.

Amphimedine (IUPAC name: 10-Methyl-8 H-benzo[b] pyrido[4,3,2-de][1,8]phenanthroline-8,11(10 H)-dione) (a marine alkaloid with the pyridoindole skeleton) exhibited a binding energy of − 9.4 kcal/mol. It shares similar core structure like neoamphimedine and followed same binding patterns with the protein. It formed one conventional hydrogen bond with Asn-1168 and two carbon-hydrogen bonds with Tyr-1125. Additionally, it established one carbon-hydrogen bond each with Phe-1111, Met-1133, and Met-1160. Amphimedine also engaged in one alkyl interaction each with Ala-1164, Val-1115, and Met-1160. Furthermore, it exhibited four, three, two, and two pi-alkyl interactions with Val-1174, Leu-1120, Pro-1110, and Val-1115, respectively. Additionally, it formed one pi-alkyl interaction each with Phe-1115, Ala-1164, and Ile-1122.

Deoxytopsentin (IUPAC name: 1 H-Indol-3-yl[5-(1 H-indol-3-yl)-1 H-imidazol-2-yl]methanone) demonstrated a binding energy of – 9.4 kcal/mol. The core structure of this compound consists of two indole rings connected through an imidazole ring. The -NH group from these sub-structures facilitated the formation of hydrogen bonds with the protein. It formed one conventional hydrogen bond each with Pro-1110, Pro-1114, and Asn-1168. Additionally, it established one carbon-hydrogen bond with Pro-1110 and one pi-sigma hydrophobic interaction with Val-1174. Furthermore, it formed three pi-alkyl interactions with Leu-1120, two pi-alkyl bonds each with Val-1115 and Val-1174, and one pi-alkyl interaction each with Pro-1110, Leu-1119, and Ala-1164.

It is important to note the diverse chemical structures of these marine lead compounds compared to the standard inhibitor, 69 A. The core structure of 69 A consists of a fused ring system made up of a benzene ring and a diazepine ring, which is a seven-membered ring containing two nitrogen atoms and one carbonyl group. Notably, the diazepine ring is absent in all of the top five marine ligands. Among these ligands, ascididemin, neoamphimedine, and amphimedine share similar structural attributes. Despite their structural differences, all five ligands interacted with key active site residues, including Pro-1110, Leu-1120, Ile-1122, Tyr-1125, Asn-1168, and Val-1174. Previous experimental reports on CREBBP bromodomain inhibition have shown that electrostatic attractions between the conserved side chains of Asn-1168, Tyr-1125, Pro-1110, and hydrophobic interactions with Ile-1122, Leu-1120, and Val-1174 are crucial for inhibitor binding and inhibition (Taylor et al. 2016; Unzue et al. 2016; Xu et al. 2016). Therefore, these marine compounds have the potential to serve as inhibitors of the bromodomain of the CBP protein.

Assessment of ADMET description

Several studies have demonstrated the significance of ADMET profile estimation in order to find potential lead or drug-like compounds that might be more tolerable during the design and development of new drugs (Bibi and Sakata 2017). Table 3 provides an overview of the ADMET characteristics of selected five compounds—stelletin A, ascididemin, neoamphimedine, amphimedine, and deoxytopsentin.

During the initial phases of drug discovery, drug-likeness is a crucial screening criterion. This parameter can be defined as a way to establish a connection between the physicochemical characteristics of a compound and its biopharmaceutical properties within the human body, particularly how they affect an oral drug's bioavailability (Bibi and Sakata 2017). For these five chosen compounds, two distinct rule-based filters, the Lipinski rule of five (Lipinski 2004) as well as the Veber's rule (Hou et al. 2007) were utilized to determine their drug-likeness. In accordance with the Lipinski Rule of Five, medications administered orally must adhere to the following criteria without exceedingly more than one of the specified limits: (i) The octanol/water partition coefficient (log P) should not exceed five, (ii) the molecular weight should be under 500 Da, (iii) there should be no more than five hydrogen bond donors, and (iv) there should be no more than 10 hydrogen bond acceptors (Lipinski 2004). On the contrary, Veber's rule indicates a compound should have equal or less than 10 rotatable bonds and a polar surface area not exceeding 140 Å2 to have good oral bioavailability (Hou et al. 2007). All five compounds conform to both Lipinski's Rule of Five and Veber's Rule, suggesting their suitability for oral drug administration. Moreover, the gastrointestinal absorption of all selected compounds is high, and both are predicted to be 55% bioavailable. Stelletin A and deoxytopsentin have a probability of crossing the BBB, but the other three compounds do not. Ascididemin is found to be moderately water-soluble, while Stelletin A, neoamphimedine, amphimedine, and deoxytopsentin have poor water solubility. However, this can be easily overcome by using appropriate formulation techniques during dosage form preparation.

Pan-Assay Interference Compounds (PAINS) are compound that produces false positive result during the initial virtual screening process of drug discovery. So, PAINS alert is utilized to rule out of them from the drug discovery steps to save time and money (Baell and Nissink 2018). All five compounds show no PAINS alert. Moreover, when considering synthetic accessibility, which is graded on a scale from 1 (indicating a very straightforward synthesis) to 10

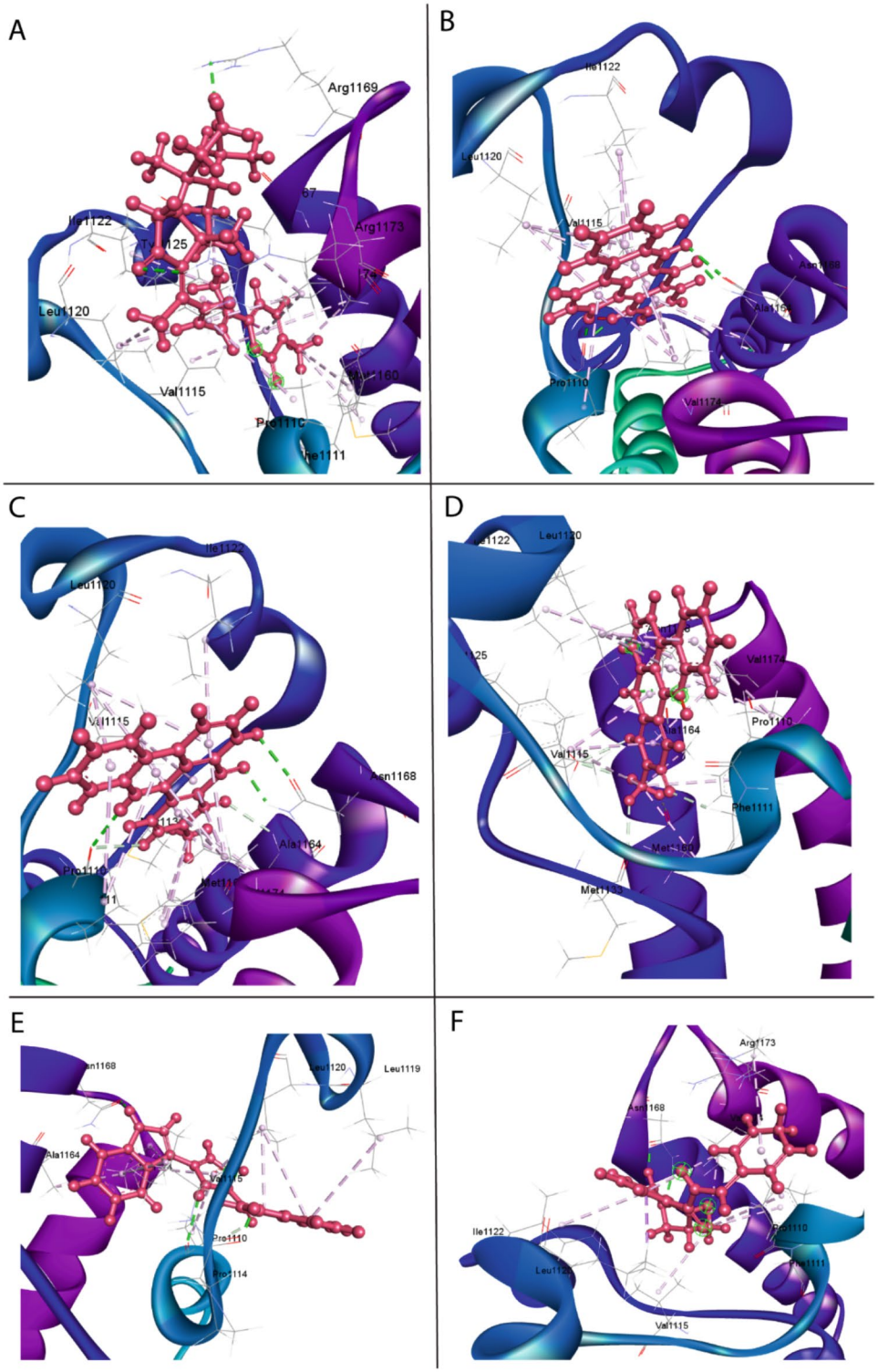

Fig. 2 Illustration of the three-dimensional molecular interactions between CBP BRD with top five marine natural compounds namely (**A**) stelletin A, (**B**) ascididemin, (**C**) neoamphimedine, (**D**) amphimedine, (**E**) deoxytopsentin, and (**F**) reference molecule, 69 A (**E**, **F**)

(representing a highly challenging synthesis), stelletin A, ascididemin, neoamphimedine, amphimedine, and deoxytopsentin exhibit synthetic accessibility values of 6.05, 2.69, 2.84, 2.80 and 2.73, respectively. This suggests that they can be readily synthesized. Throughout the drug development process, safety concerns such as toxicities and unfavourable side effects should always be considered as a necessary precondition. Nowadays, since computational methods can be performed before a compound is synthesized and are accurate, they have demonstrated significant advantages in the investigation of toxicities and adverse drug effects (Hossain et al. 2023). The ProTox II server was utilized to evaluate the toxicity of five screened compounds, and it was found that only deoxytopsentin is predicted to be hepatotoxic and mutagenic. Apart from deoxytopsentin, none of the compounds exhibited hepatotoxicity, mutagenicity, or carcinogenicity, ensuring their safety for use.

Molecular dynamics simulations

MD simulation is essential for post-dock evaluation for examining the time-dependent stability as well as the nature of motions of protein structure. MD simulations were run for 100 ns to interpret the degree of stability, flexibility, and binding behaviour of the CBP BRD (apo protein), CBP BRD-stelletin A complex, CBP BRD-ascididemin complex, CBP BRD-neoamphimedine, CBP BRD-amphimedine, CBP BRD-deoxytopsentin and CBP BRD-69 A (standard inhibitor). RMSD, RMSF, RG, SASA, and hydrogen bonding were the parameters obtained and analysed following a 100 ns MD simulations trajectory (Fig. 3) (Dutta Dubey et al. 2013).

The RMSD represents the difference between the initial structural conformation and the ultimate conformation of the protein backbone. The protein's structural conformation stability is assessed by deviations made during the simulation. Less variation in the protein backbone is seen in stable protein structures, and vice versa. For a 100 ns simulation, the RMSD value for each of the seven systems' Cα backbones was determined. From Fig. 3, it can be observed that apo protein took the first 15 ns of simulation to become stable and it lasted until 40 ns. From 40 ns to 60 ns, fluctuations of RMSD were observed but after that, it remained stable until 100 ns. CBP BRD-stelletin A complex showed stability from the beginning but fluctuations were observed from 45 ns to 57 ns similar to apo protein. After

Table 3 Molecular properties and ADMET prediction of selected five compounds

Properties	Stelletin A	Ascididemin	Neoamphimedine	Amphimedine	Deoxytopsentin
Formula	C30H38O4	C18H9N3O	C19H11N3O2	C19H11N3O2	C20H14N4O
Molecular weight	462.62 g/mol	283.28 g/mol	313.31 g/mol	313.31 g/mol	326.35 g/mol
H-bond donor	0	0	0	0	3
H-bond acceptor	4	4	4	4	2
LogP	5.97	2.62	2.26	2.25	3.24
Rotatable bonds	3	0	0	0	3
Topological polar surface area	64.35 $Å^2$	55.74 $Å^2$	64.85 $Å^2$	64.85 $Å^2$	77.33 $Å^2$
Water solubility	Poorly soluble	Moderately soluble	Poorly Soluble	Poorly Soluble	Poorly Soluble
GI absorption	High	High	High	High	High
BBB	No	Yes	Yes	Yes	No
Bioavailability score	0.55	0.55	0.55	0.55	0.55
Lipinski	Yes	Yes	Yes	Yes	Yes
Veber	Yes	Yes	Yes	Yes	Yes
PAINS	0 alert	0 alert	0 alert	0 alert	0 alert
Synthetic accessibility	6.05	2.69	2.84	2.80	2.73
Hepatotoxicity	Inactive	Inactive	Inactive	Inactive	Active
Carcinogenicity	Inactive	Inactive	Inactive	Inactive	Inactive
Mutagenicity	Inactive	Inactive	Inactive	Inactive	Active
Cytotoxicity	Inactive	Inactive	Inactive	Inactive	Inactive
Predicted LD50	800 mg/kg	2000 mg/kg	2000 mg/kg	2000 mg/kg	1264 mg/kg
Predicted Toxicity Class	4	4	4	4	4

that, it reached stability and remained stable until the end of the simulation. Both CBP BRD-ascididemin and CBP BRD-neoamphimedine complex were stable throughout the whole simulations with some minor fluctuations. Moreover, the CBP BRD-amphimedine complex remained stable until 55 ns, after which it became unstable and continued to be so until 100 ns. The CBP BRD-deoxytopsentin complex stabilized after 65 ns with an increased RMSD value. Lastly, the CBP BRD-69 A complex was stable until 45 ns, followed by a major peak between 45 and 65 ns, but eventually stabilized until the end. The apo protein, CBP BRD-stelletin A complex, CBP BRD-ascididemin complex, CBP BRD-neoamphimedine complex, CBP BRD-amphimedine complex, CBP BRD-deoxytopsentin, and CBP BRD-69 A complex had average RMSD values of 0.167, 0.149, 0.161, 0.177, 0.155, 0.186, and 0.158 nm, respectively. Therefore, stelletin A, ascididemin, and amphimedine, along with the standard inhibitor 69 A, exhibited lower average RMSD values compared to the apo protein. However, amphimedine did not maintain a stable position until the end. Thus, stelletin A and ascididemin formed relatively more stable complexes than other marine compounds, and their protein-ligand complex systems were more stable than the apo protein.

RMSF analysis determines the rigid and flexible regions of the protein as well as protein-ligand complexes. In order to estimate the structural alterations in protein structure brought on by ligand binding, we calculated the RMSF value. The N-terminal of protein showed higher fluctuations in all systems (Fig. 3). All seven systems produced similar graphs, with a small region of amino acid residues ranging from 1117 to 1127 showing higher flexibility. Within this region, ascididemin and neoamphimedine exhibited relatively lower RMSF values compared to the other systems. The CBP BRD-deoxytopsentin system demonstrated higher RMSF values across most amino acids, which accounts for its higher RMSD value. The average RMSF values for the apo protein, CBP BRD-stelletin A complex, CBP BRD-ascididemin complex, CBP BRD-neoamphimedine complex, CBP BRD-amphimedine complex, CBP BRD-deoxytopsentin, and CBP BRD-69 A complex were 0.11, 0.10, 0.08, 0.08, 0.08, 0.11, and 0.09 nm, respectively. So, these ligands binding reduced flexibility of the protein which indicated that the compounds formed a stable complex by fitting well in the protein's active site except deoxytopsentin.

Rg is utilized to examine the compactness and overall stability of the proteins before and after ligand binding throughout the simulation. The average Rg values for the apo protein, CBP BRD-stelletin A complex, CBP BRD-ascididemin complex, CBP BRD-neoamphimedine complex, CBP BRD-amphimedine complex, CBP BRD-deoxytopsentin, and CBP BRD-69 A complex were 1.50, 1.50, 1.49, 1.51, 1.49, 1.50, and 1.48 nm, respectively. Upon analyzing the results, it was found that the Rg values for all ligand complexes, except for deoxytopsentin, were lower than that of the apo protein. The CBP BRD-ascididemin and BRD-amphimedine complexes exhibited the most stable protein structures (Fig. 3).

Another crucial parameter under scrutiny was SASA, which was explored to determine the degree of the protein surface that can be reached by water molecules (Fig. 3). Reduced SASA values signify limited expansion and thus greater structural compactness in the protein. The apo protein, CBP BRD-stelletin A complex, CBP BRD-ascididemin complex, CBP BRD-neoamphimedine complex, CBP BRD-amphimedine complex, CBP BRD-deoxytopsentin, and CBP BRD-69 A complex were shown to have average SASA values of 77.03, 77.82, 76.77, 78.03, 76.67, 76.82, and 76.52 nm^2, respectively. These results suggest that there are no significant differences between the apo protein and their ligand-bound structures. Supporting the findings from the Rg parameter analysis, the CBP BRD-ascididemin and BRD-amphimedine complexes displayed the lowest SASA values, indicating the lowest expansion and highest compactness of the protein. Based on the above discussion, the stability of the apo protein and their complexes during the simulation was confirmed by the SASA analysis results.

The hydrogen bond interactions serve a crucial part in the stabilization of the protein-ligand complex. The average number of hydrogen bonds formed by the CBP BRD-stelletin A complex, CBP BRD-ascididemin complex, CBP BRD-neoamphimedine complex, CBP BRD-amphimedine complex, CBP BRD-deoxytopsentin, and CBP BRD-69 A complex were 0.59, 2.03, 2.26, 2.33, and 0.73, respectively. The range of hydrogen bond formation for stelletin A, ascididemin, neoamphimedine, amphimedine, deoxytopsentin, and 69 A were 0–3, 0–4, 0–4, 0–5, 0–4, and 0–6, respectively. This data indicates that these ligands and the protein can form stable complexes.

PCA was utilized to evaluate the conformational space and transition dynamics of seven systems: the apo protein, CBP BRD-stelletin A complex, CBP BRD-ascididemin complex, CBP BRD-neoamphimedine complex, CBP BRD-amphimedine complex, CBP BRD-deoxytopsentin, and CBP BRD-69 A complex. This statistical method aims to simplify the MD simulation trajectory data complexity by isolating the collective motion of Cα backbone atoms. This approach retains the crucial variations necessary for assessing complex stability while reducing overall complexity (Sharma et al. 2022). The 2D projection of trajectories for the major principal components PC1 and PC2 of these seven systems is depicted in Fig. 4, illustrating distinct conformations in 2D space.

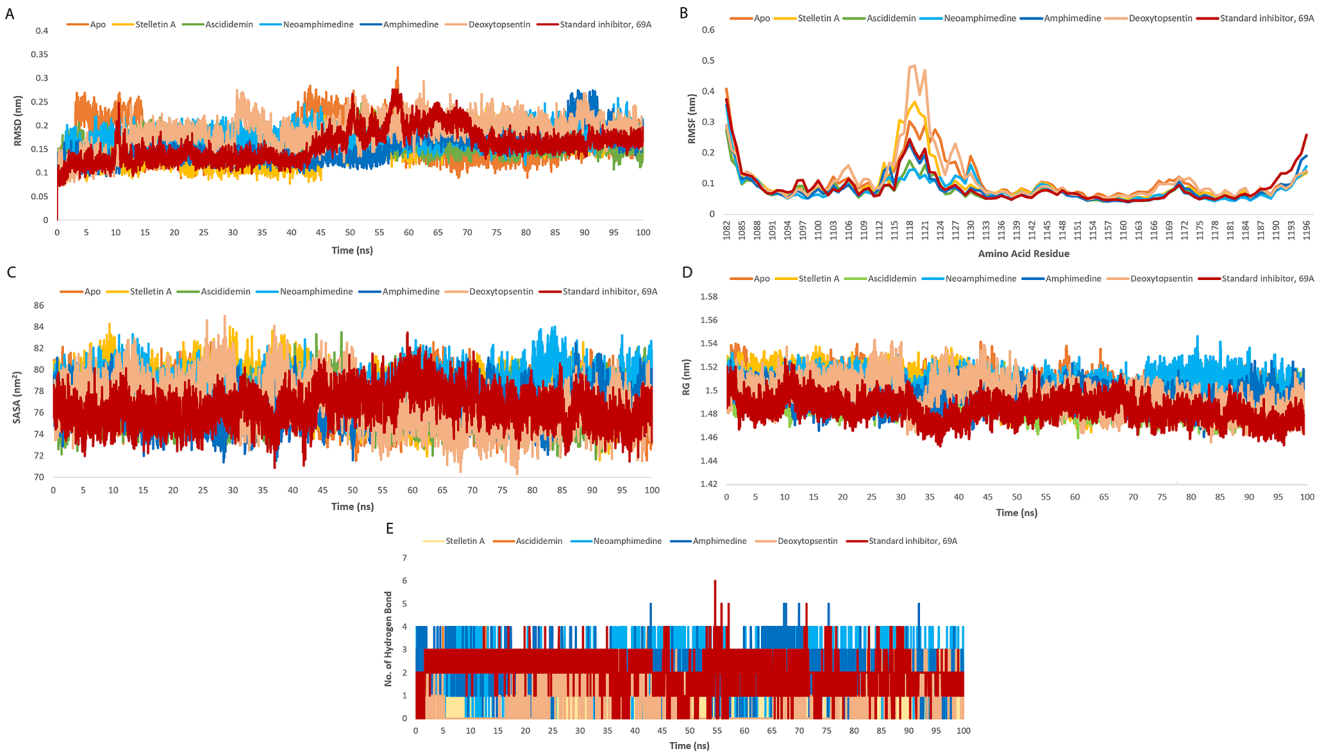

Fig. 3 MD simulation result of CBP BRD (apo protein), CBP BRD-stelletin A complex, CBP BRD-ascididemin complex, CBP BRD-neoamphimedine, CBP BRD-amphimedine, CBP BRD-deoxytopsentin and CBP BRD-69 A (standard inhibitor). (**A**) RMSD, (**B**) RMSF, (**C**) SASA, (**D**) Radius of gyration, (**E**) intermolecular hydrogen bonds represent the structural changes and flexibility of the seven systems. The colors represented CBP BRD, CBP BRD-stelletin A complex, CBP BRD-ascididemin, CBP BRD-neoamphimedine, CBP BRD-amphimedine, CBP BRD-deoxytopsentin and CBP BRD-69 A (standard inhibitor) complex in A, B, C, D, and E are yellow, orange, sky blue, blue, cream and brown respectively

In this representation, well-defined and less space-occupying clusters signify stable complexes, while more space-occupying clusters denote unstable complexes.

PCA revealed that most of the protein-ligand complexes formed noticeably less space-occupying clusters and exhibited reduced motions compared to the free-state of the CBP BRD, indicating increased stability post-ligand binding. Notably, the CBP BRD-ascididemin complex exhibited the least movement and produced a compact, less space-occupying cluster, suggesting superior stability among the seven systems. The flexibility of all protein-inhibitor complexes was assessed by computing the trace value for the diagonalized covariance matrix, representing the sum of eigenvalues. Higher trace values indicate increased flexibility. The trace values for apo protein, CBP BRD-stelletin A complex, CBP BRD-ascididemin complex, CBP BRD-neoamphimedine complex, CBP BRD-amphimedine complex, CBP BRD-deoxytopsentin, and CBP BRD-69 A complex were 1.767, 1.561, 0.822, 0.951, 1.030, 2.228 and 1.272 nm², respectively. Therefore, the apo protein displayed the highest flexibility in comparison to its ligand-bound state except CBP BRD-deoxytopsentin complex, while the CBP BRD-ascididemin complex exhibited the least flexibility, signifying greater stability. These PCA results align with conclusions drawn from other analyses such as RMSD, RMSF, SASA, and RG.

FELs play a crucial role in investigating the conformational changes in proteins and their functions. An FEL serves as a representation of every conceivable conformation of biological macromolecules such as proteins (Wang et al. 2023). It illustrates the process of a protein folding and unfolding as it progresses toward its native state and attains global minima. Additionally, FEL aids in comprehending the range of conformational variations while considering energy minimization. The analysis of the Gibbs free energy landscape was carried out by utilizing the first two principal components (Fig. 5) (Altis et al. 2008).

In Fig. 5, the deepest blue shade represents the protein's conformation with the lowest energy, while the red shade signifies the conformation with the highest energy state. The profound well indicates a thermodynamically favourable state for the proteins. We calculated the FEL for CBP BRD

in its apo state and its associated protein–ligand complexes. The ΔG values for the apo protein ranged from 0 kJ/mol to − 13.9 kJ/mol, and For the CBP BRD-stelletin A complex, CBP BRD-ascididemin complex, CBP BRD-neoamphimedine complex, CBP BRD-amphimedine complex, CBP BRD-deoxytopsentin complex, and CBP BRD-69 A complex, the ΔG values ranged from 0 kJ/mol to − 12.7 kJ/mol, 0 kJ/mol to − 12.5 kJ/mol, 0 kJ/mol to − 13.5 kJ/mol, 0 kJ/mol to − 13.8 kJ/mol, 0 kJ/mol to − 15 kJ/mol, and 0 kJ/mol to − 14 kJ/mol, respectively. These results suggest that the most of the ligand-bound state of the protein are energetically more favorable than the apo state, and these compounds formed stable protein-ligand complexes with the bromodomain of CBP.

Analysing the FELs reveals that both the apo protein and the CBP BRD-stelletin A complex exhibit two energy funnels separated by distinct energy barriers, each having 2–3 energy minima (Fig. 5A, B). From these two systems, the energy funnels associated with the CBP BRD-stelletin A complex have a more pronounced blue-coloured central valley, indicating that the protein in this complex can adopt two distinct conformational states. Additionally, the CBP BRD-amphimedine complex, CBP BRD-deoxytopsentin complex, and CBP BRD-69 A complex exhibited multiple funnels separated by distinct energy barriers, each containing several energy minima. In contrast, the CBP BRD-ascididemin complex (Fig. 5C) and CBP BRD-neoamphimedine complex (Fig. 5D) showed a single funnel with a single, larger global minimum. This indicates that these complexes have one predominant, highly stable conformation and are more stable than the other systems.

Based on the preceding analysis, it is notable that during MD simulations, stelletin A, ascididemin, and neoamphimedine demonstrated superior stability and formed more stable complexes compared to other marine compounds.

Cluster analysis

To explore the conformational diversity in complex structures and protein structures that exhibit similarity throughout the entire MD simulation trajectory, we conducted clustering analysis using the Gromos clustering algorithm with a Cα-RMSD cutoff of 0.15 nm. Figure 6 illustrates the visual representation of all representative structures from each cluster for all seven systems.

Analysis of conformational variability revealed distinct patterns. The apo protein demonstrated the highest degree of flexibility with eleven clusters and RMSD values spanning 0.046 to 0.483 nm (average 0.087 nm). In contrast, the CBP BRD-ascididemin complex exhibited the least conformational diversity with three clusters and RMSD values ranging from 0.04 to 0.316 nm (average 0.084 nm).

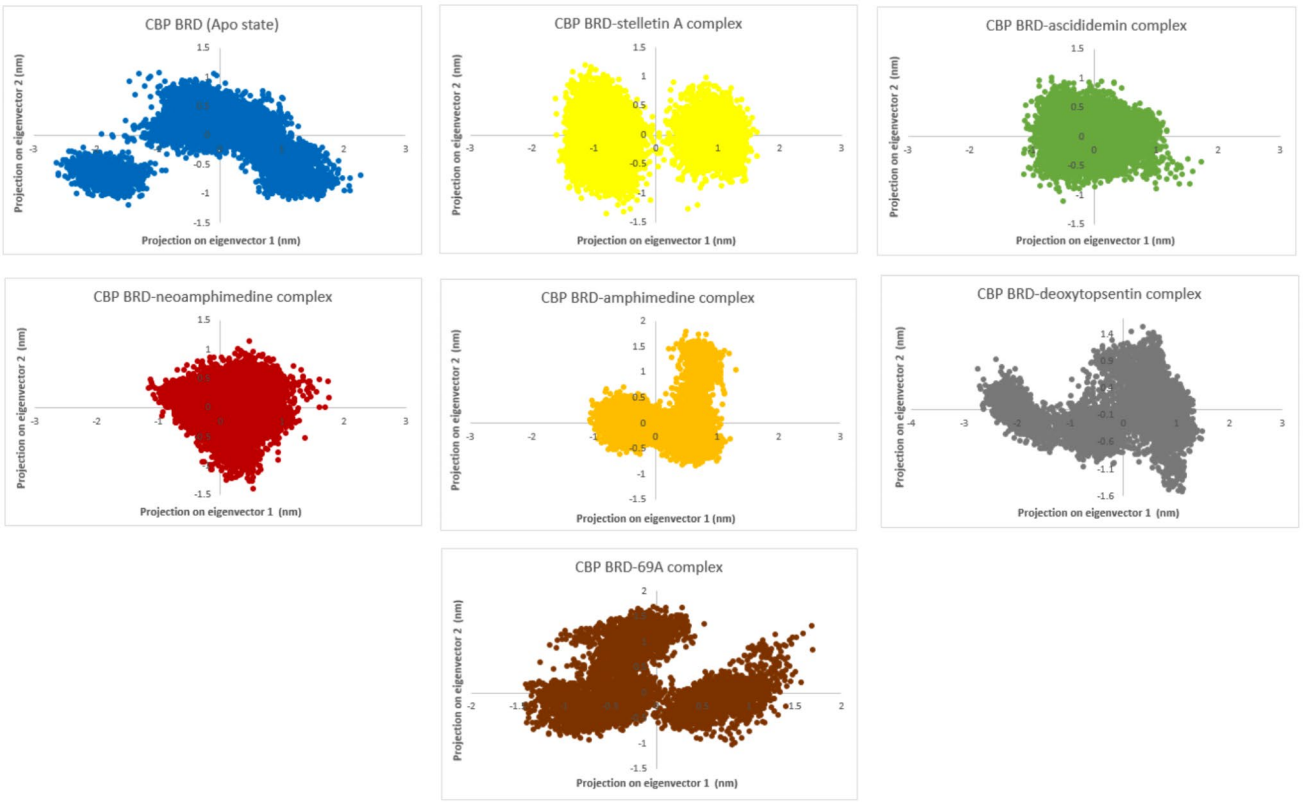

Fig. 4 Principal component analyses of CBP's bromodomain in apo state as well as ligand bound state

The remaining complexes showed intermediate levels of flexibility, with stelletin A forming four clusters (RMSD: 0.044–0.341 nm, average 0.087 nm), neoamphimedine and amphimedine forming five clusters each (neoamphimedine: RMSD 0.043–0.321 nm, average 0.083 nm; amphimedine: RMSD 0.044–0.285 nm, average 0.084 nm), and 69 A forming seven clusters (RMSD 0.044–0.366 nm, average 0.084 nm). Deoxytopsentin displayed a conformational landscape similar to the apo protein, with eleven clusters but a slightly narrower RMSD range of 0.040–0.447 nm (average 0.118 nm).

As anticipated, the ligand-bound proteins showed a lower number of clusters compared to the apo protein, indicating increased stability post-ligand binding and less flexible dynamics in these complexes. These observations are consistent with the results obtained from RMSF and PCA. Therefore, it can be concluded that theses marine compounds except deoxytopsentin formed relatively stable protein-ligand complexes with CBP BRD.

It is noteworthy that the segment of the protein encompassing amino acids Val-1115 to Lys-1130 displayed higher flexibility compared to the remaining protein structures (Fig. 6). This pattern was consistent across all seven systems, suggesting that these specific regions play a role in the adoption of varied conformations by the protein structures associated with all seven systems. While other regions remained relatively stable, the mentioned segment significantly contributed to the overall movement, flexibility, and dynamic nature of the protein structures. This observation aligns with the outcomes obtained from the RMSF analysis.

MM-PBSA calculation

The MM-PBSA method, which is integrated into the g_mmpbsa tool, was utilized to measure the binding free energy (ΔG_{bind}) of stelletin A, ascididemin, neoamphimedine, amphimedine, deoxytopsentin as well as standard inhibitor, 69 A with the protein. The final 10 ns of the 100 ns MD simulation trajectories were utilized to calculate the ΔG_{bind}, which is primarily controlled by non-covalent forces. Primarily, non-covalent forces play a pivotal role in stabilizing protein-ligand interactions, encompassing electrostatic interactions, hydrophobic interactions, hydrogen bonds, and van der Waals forces. These forces can either enhance or diminish the overall binding, depending on their specific contributions. The MM-PBSA method provided the

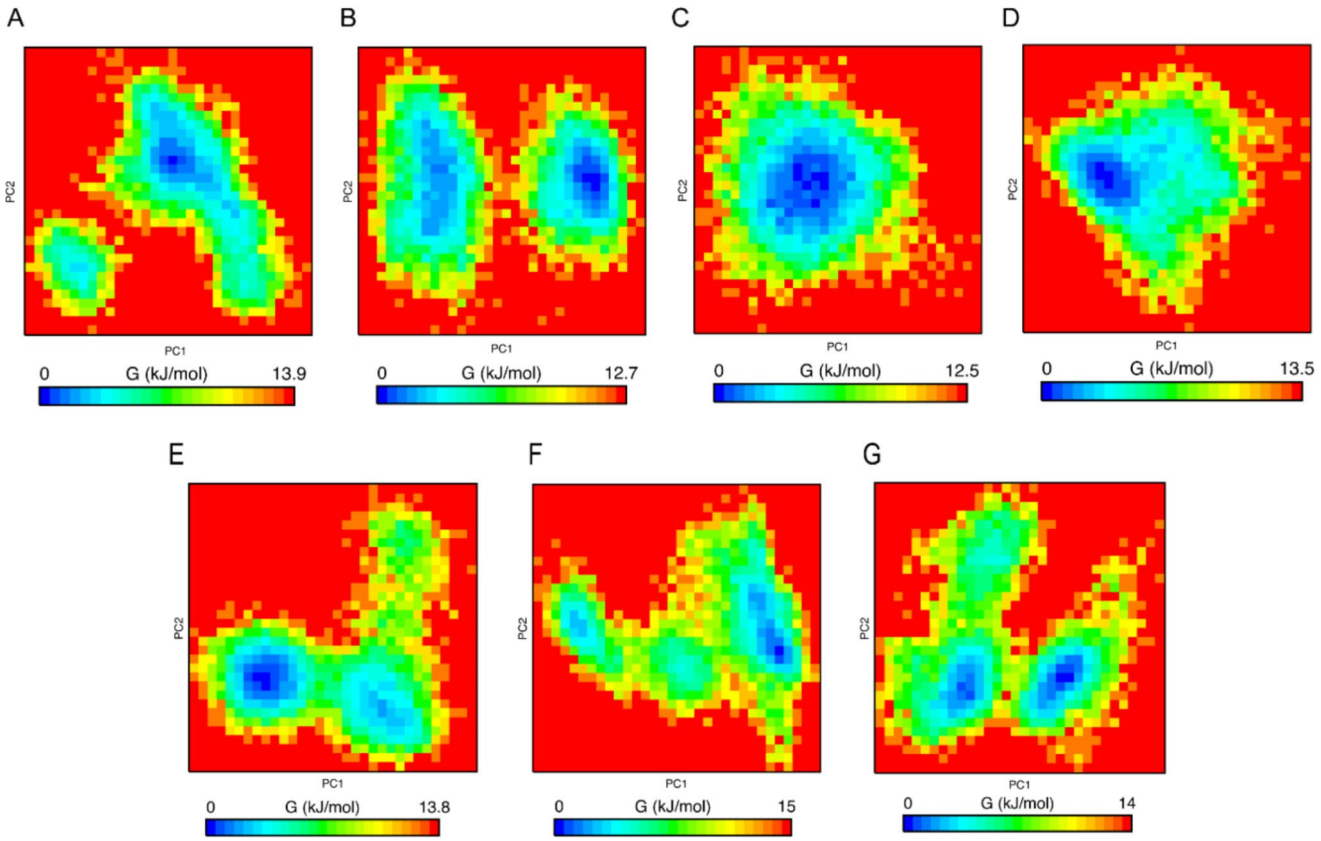

Fig. 5 Free energy landscape of the first two principal components for CBP's bromodomain (**A**) CBP BRD in apo state, (**B**) CBP BRD-stelletin A complex (**C**) CBP BRD-ascididemin complex, (**D**) CBP BRD-neoamphimedine complex, (**E**) CBP BRD-amphimedine complex, (**F**) CBP BRD-deoxytopsentin, and (**G**) CBP BRD-69 A complex

computed results for the van der Waals, electrostatic, polar solvation, solvent-accessible surface area (SASA), and binding free energies, as shown in Table 4 as well as illustrated in Fig. 6A.

According to the MM-PBSA calculations, the total ΔG_{bind} of the protein and standard inhibitor, 69 A was found to be approximate -77.191 ± 15.904 kJ/mol. From the five-marine compound, three of them showed lower ΔG_{bind} compared to 69 A. Ascididemin showed lowest total ΔG_{bind} of -152.656 ± 48.692 kJ/mol followed by neoamphimedine (-85.160 ± 12.817 kJ/mol) and stelletin A (-79.694 ± 32.073 kJ/mol). In all six complexes, the maximum contributor for complex formation was the electrostatic energy. The results clearly demonstrate that these compounds specially ascididemin, neoamphimedine and stelletin A exhibit substantial affinity for the protein.

The MM-PBSA data was further employed to pinpoint the primary residues that made the most substantial contributions to the binding (Fig. 7). For stelletin A's interaction with the bromodomain of CREBBP, the key energy-contributing residues were Leu-1109, Pro-1110, Val-1174, Leu-1120, Tyr-1167, Ile-1122, Arg-1112, Phe-1111, Gln-1113, Lys-1176, Val-1115, Arg-1169, Phe-1177, Asp-1116, and Tyr-1125. In contrast, the critical energy-contributing residues for the interaction between ascididemin and the CREBBP bromodomain included Asp-1124, Asp-1127, Asp-1116, Asp-1134, Asp-1156, Asp-1155, Glu-1107, Asp-1105, Glu-1186, Glu-1183, Glu-1149, Asp-1143, Glu-1099, Glu-1188, Asp-1190, Leu-1196, Glu-1088, Glu-1089, and Tyr-1167. Moreover, the key energy-contributing residues for neoamphimedine's interaction with the bromodomain of CREBBP were Met-1133, Arg-1173, Tyr-1125, Lys-1139, Arg-1140, and Arg-1112. On the other hand, the critical energy-contributing residues for the interaction between the standard inhibitor 69 A and the CREBBP bromodomain included Asp-1124, Asp-1116, Asp-1105, Asp-1134, Glu-1107, Asp-1127, Glu-1099, Asp-1156, Glu-1183, Asp-1155, Glu-1186, Asp-1143, Glu-1188, Asp-1190, Glu-1149,

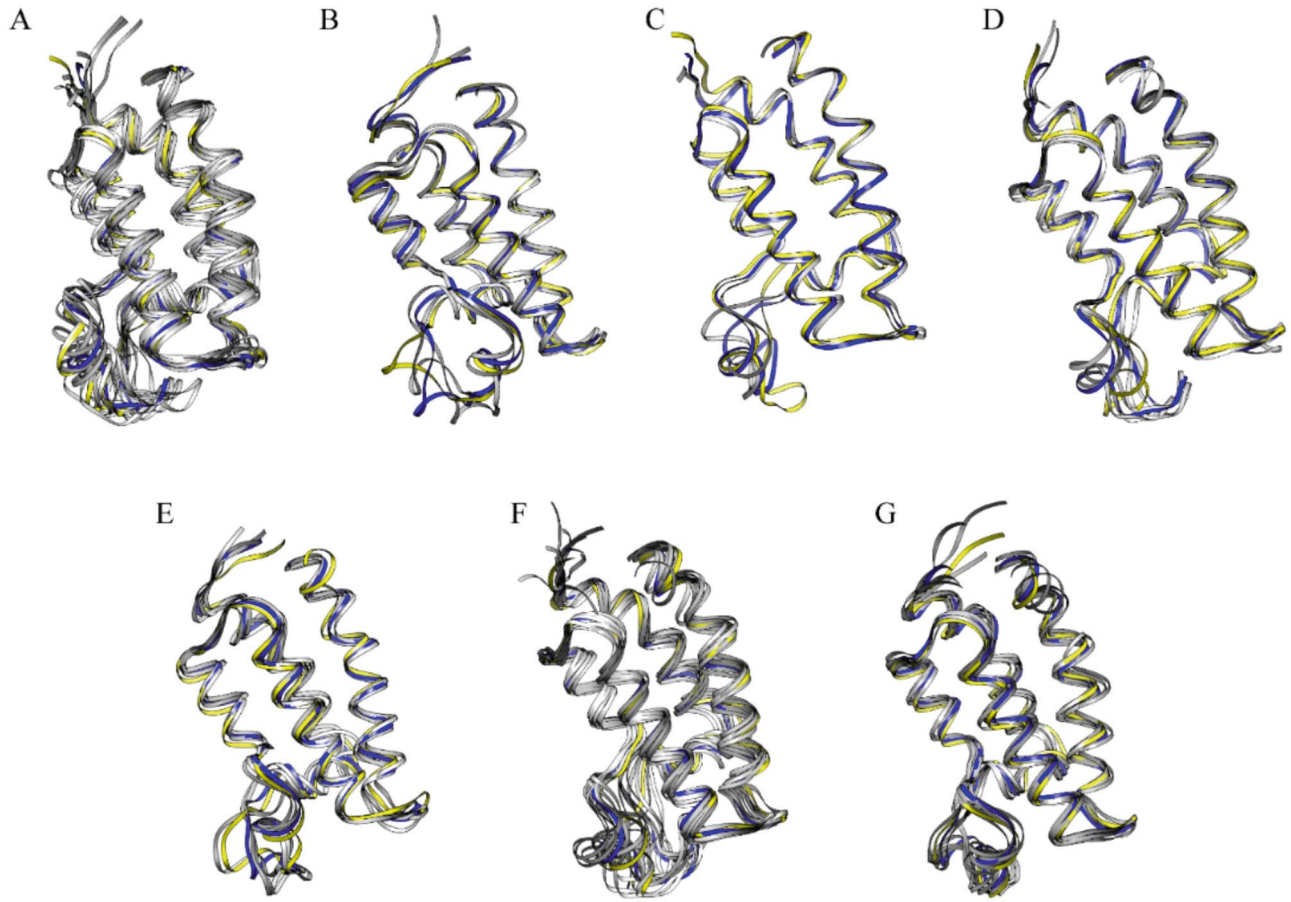

Fig. 6 Visualization of the central conformation, which serves as a representative of the average structure within each cluster, is presented for CBP's bromodomain in both the apo and ligand-bound states during MD simulation where blue and yellow color represents the representative structure of 1st and 2nd cluster respectively. Superimposition is performed for all clusters of (**A**) the apo protein, (**B**) CBP BRD-Stelletin A complex, (**C**) CBP BRD-ascididemin complex, (**D**) CBP BRD-neoamphimedine complex, (**E**) CBP BRD-amphimedine complex, (**F**) CBP BRD-deoxytopsentin, and (**G**) CBP BRD-69 A complex

Table 4 Van Der Waal's, electrostatic, polar salvation, SASA as well as binding free energy of top five selected compounds in kJ/mol

Compound	van der Waals energy	Electrostatic energy	Polar solvation energy	SASA energy	Binding free energy
Ascididemin	26.28 ± 15.360	− 884.277 ± 124.195	709.48 ± 147.136	− 4.139 ± 1.225	− 152.656 ± 48.692
Neoamphimedine	− 170.959 ± 11.221	− 50.653 ± 7.923	153.551 ± 11.488	− 17.099 ± 0.869	− 85.160 ± 12.817
Stelletin A	− 105.139 ± 16.174	− 28.655 ± 10.033	68.186 ± 36.018	− 14.086 ± 1.549	− 79.694 ± 32.073
Amphimedine	− 152.426 ± 9.765	− 31.099 ± 7.106	128.639 ± 11.322	− 15.416 ± 0.824	− 69.301 ± 10.563
Deoxytopsentin	− 94.114 ± 10.483	− 68.489 ± 20.422	144.996 ± 40.349	− 12.251 ± 1.132	− 29.859 ± 36.918
Standard inhibitor, 69 A	− 77.333 ± 13.897	− 82.788 ± 26.220	93.724 ± 30.234	− 10.794 ± 1.629	− 77.191 ± 15.904

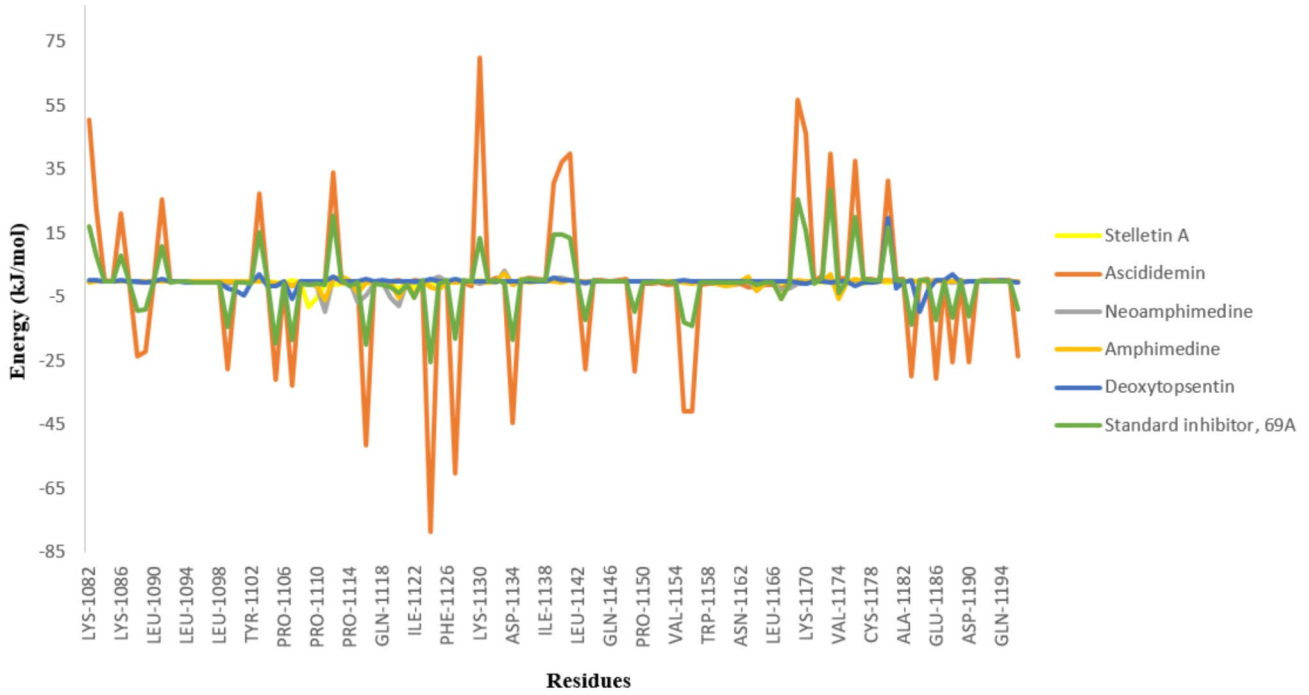

Fig. 7 Residues with free energy contribution of CBP BRD with stelletin A, ascididemin, neoamphimedine, amphimedine, and deoxytopsentin

Glu-1088, Leu-1196, Glu-1089, Tyr-1167, Ile-1122, Leu-1120, Val-1174, Leu-1119, Pro-1114, and Gly-1121.

In silico PASS prediction

The PASS program forecasts the biological properties of small molecules based on structure-activity relationships of large sets of compound datasets. This tool assists in the exploration of highly effective and novel medicinal compounds. Based on the analyses above, we found that three specific marine compounds—stelletin A, ascididemin, and neoamphimedine—formed stable complexes with the bromodomain of CBP, exhibiting high binding affinities. Therefore, we investigated their anticancer properties using PASS prediction.

According to this tool, ascididemin showed high probabilities (0.831/0.009) for antineoplastic predictions and was particularly promising for antineoplastic applications in colorectal cancer (0.806/0.004) and bladder cancer (0.777/0.002). Stelletin A exhibited elevated likelihoods for antineoplastic (0.951/0.004), antileukemic (0.869/0.004), and apoptosis agonist (0.845/0.005) predictions. Additionally, neoamphimedine also demonstrated higher probabilities (0.747/0.019) for antineoplastic predictions and was particularly promising for antineoplastic applications in colorectal cancer (0.740/0.005) and bladder cancer (0.719/0.005), like ascididemin. These results indicated that these three marine compounds have high anticancer potential.

Conclusion

The bromodomain of CBP acts as an epigenetic reader in cells and is an important drug target for finding safe and effective anticancer agents. In this study, we utilized molecular docking, ADMET study, MD simulation, MM-PBSA approach, and in silico PASS prediction to find effective inhibitors of CBP BRD from marine-derived natural compounds. Marine compounds are known for their distinctive

chemical compositions and exhibit greater effectiveness in fighting cancer compared to plant-based compounds from the land. Molecular docking analysis revealed that five marine compounds—stelletin A (-10.1 kcal/mol), ascididemin (-10.1 kcal/mol), neoamphimedine (-10 kcal/mol), amphimedine (-9.4 kcal/mol), and deoxytopsentin (-9.4 kcal/mol)—exhibited significantly higher binding affinities than the known standard inhibitor, benzodiazepinone G02778174 (-8.8 kcal/mol). Further evaluation of their ADMET properties suggested that these compounds, with the exception of deoxytopsentin, would be safe for use as drugs without causing toxicity or cancer. Molecular dynamics simulations of the five ligand-protein complexes showed that all compounds, except deoxytopsentin, formed stable complexes with the protein. Additionally, MM-PBSA calculations indicated that ascididemin, neoamphimedine, and stelletin A had lower binding free energies with the protein, resulting in more stable protein-ligand complexes. Among these, ascididemin exhibited significantly higher binding free energy with the CBP BRD than the other marine compounds and the standard inhibitor. According to the PASS tool, ascididemin, neoamphimedine, and stelletin A also have strong anticancer potential. Thus, the marine-derived compound, ascididemin has the potential to be a CBP BRD inhibitor, contributing to the advancement of prospective anticancer medications. In the future, its efficacy in targeting the CBP BRD should be assessed through both in vitro and in vivo experiments.

Supplementary Information The online version contains supplementary material available at https://doi.org/10.1007/s40203-024-00258-5.

Acknowledgements Not applicable.

Author contributions MLA: conceptualization and supervision of the project. FN: preparing compound library and performing molecular docking study. EA and MMH: performing the molecular dynamics simulations and MM-PBSA analysis. NH: performing the ADMET analysis and in silico PASS prediction study. AFM: Performing the illustration and data analysis. MLA wrote the whole manuscript. All authors reviewed the manuscript.

Funding This research did not receive any kind of funding.

Data availability No datasets were generated or analysed during the current study.

Declarations

Competing interests The authors declare no competing interests.

References

Abraham MJ, Murtola T, Schulz R, Páll S, Smith JC, Hess B et al (2015) GROMACS: high performance molecular simulations through multi-level parallelism from laptops to supercomputers. SoftwareX Elsevier 1:19–25

Acharya R, Chacko S, Bose P, Lapenna A, Pattanayak SP (2019) Structure based multitargeted molecular docking analysis of selected furanocoumarins against breast cancer. Sci Rep Nat Publishing Group UK Lond 9(1):15743

Ali L, Roky AH, Azad AK, Shaikat AH, Meem JN, Hoque E et al (2024a) Autophagy as a targeted therapeutic approach for skin cancer: evaluating natural and synthetic molecular interventions. Cancer Pathogenesis and Therapy. Chinese Medical Association Publishing House Co., Ltd 42 Dongsi Xidajie 2:E01–E57

Ali ML, Noushin F, Sadia QA, Metu AF, Meem JN, Chowdhury MT et al (2024b) Spices and culinary herbs for the prevention and treatment of breast cancer: a comprehensive review with mechanistic insights. Cancer Pathogenesis and Therapy. Chinese Medical Association Publishing House Co., Ltd 42 Dongsi Xidajie 2:E082–E142

Altis A, Otten M, Nguyen PH, Hegger R, Stock G (2008) Construction of the free energy landscape of biomolecules via dihedral angle principal component analysis. J Chem Phys AIP Publishing 128(24):245102

Armstrong AJ, Gordon MS, Reimers MA, Hussain A, Patel VG, Lam ET et al (2021) Abstract P202: initial findings from an ongoing first-in-human phase 1 study of the CBP/p300 inhibitor FT-7051 in men with metastatic castration-resistant prostate cancer. Mol Cancer Ther AACR 20(12Supplement):P202–P202

Baell JB, Nissink JWM (2018) Seven Year Itch: Pan-assay Interference compounds (PAINS) in 2017 Utility and limitations. ACS Chem Biol ACS Publications 13(1):36–44

Banerjee P, Eckert AO, Schrey AK, Preissner R (2018) ProTox-II: a webserver for the prediction of toxicity of chemicals. Nucleic Acids Res. Oxford University Press 46(W1):W257–63

Barreca M, Spanò V, Montalbano A, Cueto M, Díaz Marrero AR, Deniz I et al (2020) Marine anticancer agents: an overview with a particular focus on their chemical classes. Mar Drugs MDPI 18(12):619

Bibi S, Sakata K (2017) An integrated computational approach for plant-based protein tyrosine phosphatase non-receptor type 1 inhibitors. Curr Comput Aided Drug Des Bentham Sci Publishers 13(4):319–335

Bjelkmar P, Larsson P, Cuendet MA, Hess B, Lindahl E (2010) Implementation of the CHARMM force field in GROMACS: analysis of protein stability effects from correction maps, virtual interaction sites, and water models. J Chem Theory Comput ACS Publications 6(2):459–466

Bugnon M, Goullieux M, Röhrig UF, Perez MAS, Daina A, Michielin O et al (2023) SwissParam 2023: A Modern Web-Based Tool for Efficient Small Molecule Parametrization. J Chem Inf Model. ACS Publications

Chekler ELP, Pellegrino JA, Lanz TA, Denny RA, Flick AC, Coe J et al (2015) Transcriptional profiling of a selective CREB binding protein bromodomain inhibitor highlights therapeutic opportunities. Chem Biol Elsevier 22(12):1588–1596

Chtita S, Fouedjou RT, Belaidi S, Djoumbissie LA, Ouassaf M, Qais FA et al (2022) In silico investigation of phytoconstituents from Cameroonian medicinal plants towards COVID-19 treatment. Struct Chem Springer 33(5):1799–1813

Conery AR, Centore RC, Neiss A, Keller PJ, Joshi S, Spillane KL et al (2016) Bromodomain inhibition of the transcriptional coactivators CBP/EP300 as a therapeutic strategy to target the IRF4 network in multiple myeloma, vol 5. Elife. eLife Sciences Publications, Ltd, p e10483

Daina A, Michielin O, Zoete V (2017) SwissADME: a free web tool to evaluate pharmacokinetics, drug-likeness and medicinal chemistry friendliness of small molecules. Sci Rep Nat Publishing Group UK Lond 7(1):42717

Dallakyan S, Olson AJ (2015) Small-molecule library screening by docking with PyRx. Methods Mol Biol 1263:243–50

Dancy BM, Cole PA (2015) Protein lysine acetylation by p300/CBP. Chem Rev ACS Publications 115(6):2419–2452

Daoui O, Mali SN, Elkhattabi K, Elkhattabi S, Chtita S (2023) Repositioning cannabinoids and terpenes as Novel EGFR-TKIs candidates for targeted Therapy Against Cancer: a virtual screening model using CADD and biophysical simulations. Heliyon 9(4):e15545

Das C, Roy S, Namjoshi S, Malarkey CS, Jones DNM, Kutateladze TG et al (2014) Binding of the histone chaperone ASF1 to the CBP bromodomain promotes histone acetylation. Proceedings of the National Academy of Sciences. National Acad Sciences 111(12):E1072–81

Dash R, Mitra S, Arifuzzaman M, Zahid Hosen SM (2018) In silico quest of selective naphthyl-based CREBBP bromodomain inhibitor. Silico Pharmacol Springer 6:1–10

Dassonneville L, Wattez N, Baldeyrou B, Mahieu C, Lansiaux A, Banaigs B et al (2000) Inhibition of topoisomerase II by the marine alkaloid ascididemin and induction of apoptosis in leukemia cells. Biochem Pharmacol Elsevier 60(4):527–537

Daura X, Gademann K, Jaun B, Seebach D, Van Gunsteren WF, Mark AE (1999) Peptide folding: when simulation meets experiment. Angewandte Chemie Int Ed Wiley Online Libr 38(1–2):236–240

De Guzman FS, Carte B, Troupe N, Faulkner DJ, Harper MK, Concepcion GP et al (1999) Neoamphimedine: a new pyridoacridine topoisomerase II inhibitor which catenates DNA. Journal of organic chemistry, vol 64. ACS American Chemical Society, pp 1400–1402

Dutta Dubey K, Kumar Tiwari R, Prasad Ojha R (2013) Recent advances in protein–ligand interactions: molecular dynamics simulations and binding free energy. Curr Comput Aided Drug Des Bentham Sci Publishers 9(4):518–531

Ebada SS, Lin W, Proksch P (2010) Bioactive sesterterpenes and triterpenes from marine sponges: occurrence and pharmacological significance. Mar Drugs Mol Divers Preservation Int 8(2):313–346

Eberhardt J, Santos-Martins D, Tillack AF, Forli S (2021) AutoDock Vina 1.2. 0: new docking methods, expanded force field, and python bindings. J Chem Inf Model ACS Publications 61(8):3891–3898

Ghosh S, Taylor A, Chin M, Huang H-R, Conery AR, Mertz JA et al (2016) Regulatory T cell modulation by CBP/EP300 bromodomain inhibition. J Biol Chem ASBMB 291(25):13014–13027

Guex N, Peitsch MC (1997) SWISS-MODEL and the Swiss-pdb viewer: an environment for comparative protein modeling. Electrophoresis Wiley Online Libr 18(15):2714–2723

Gupta L, Talwar A, Chauhan PMS (2007) Bis and tris indole alkaloids from marine organisms: new leads for drug discovery. Curr Med Chem Bentham Sci Publishers 14(16):1789–1803

Hossain A, Rahman ME, Rahman MS, Nasirujjaman K, Matin MN, Faruqe MO et al (2023) Identification of medicinal plant-based phytochemicals as a potential inhibitor for SARS-CoV-2 main protease (Mpro) using molecular docking and deep learning methods. Comput Biol Med 157:106785

Hou T, Wang J, Zhang W, Xu X (2007) ADME evaluation in drug discovery. 6. Can oral bioavailability in humans be effectively predicted by simple molecular property-based rules? J Chem Inf Model ACS Publications 47(2):460–463

Jiménez C (2018) Marine natural products in medicinal chemistry. ACS Med Chem Lett. ACS Publications pp. 959–61

Kar B, Kundu CN, Pati S, Bhattacharya D (2023) Discovery of phytocompounds as novel inhibitors against NDM-1 and VIM-1 protein through virtual screening and molecular modelling. J Biomol Struct Dyn Taylor Francis 41(4):1267–1280

Khalifa SAM, Elias N, Farag MA, Chen L, Saeed A, Hegazy M-EF et al (2019) Marine natural products: a source of novel anticancer drugs. Mar Drugs MDPI 17(9):491

Knurowski T, Clegg K, Brooks N, Ashby F, Pegg NA, West W et al (2019) An open-label phase I/IIa study to evaluate the safety and efficacy of CCS1477, a first in clinic inhibitor of the p300/CPB Bromodomains, as Monotherapy in patients with Advanced Haematological malignancies. Blood Elsevier 134:1266

Kumari R, Kumar R, Consortium OSDD, Lynn A (2014) g_mmpbsa—a GROMACS tool for high-throughput MM-PBSA calculations. J Chem Inf Model 54(7):1951–1962

Lagunin A, Stepanchikova A, Filimonov D, Poroikov V (2000) PASS: prediction of activity spectra for biologically active substances. Bioinformatics, vol 16. Oxford University Press, pp 747–748. 8

Li D-D, Guo J-F, Huang J-J, Wang L-L, Deng R, Liu J-N et al (2010) Rhabdastrellic acid-A induced autophagy-associated cell death through blocking Akt pathway in human cancer cells. PLoS One. Public Library of Science San Francisco, USA 5(8):e12176

Lipinski CA (2004) Lead-and drug-like compounds: the rule-of-five revolution. Drug Discov Today Technol Elsevier 1(4):337–341

Lokhande KB, Doiphode S, Vyas R, Swamy KV (2021) Molecular docking and simulation studies on SARS-CoV-2 Mpro reveals Mitoxantrone, Leucovorin, Birinapant, and Dynasore as potent drugs against COVID-19. J Biomol Struct Dyn Taylor Francis 39(18):7294–7305

Lokhande KB, Banerjee T, Swamy KV, Ghosh P, Deshpande M (2022) An in silico scientific basis for LL-37 as a therapeutic for Covid-19. Proteins 90(5):1029–1043

Macalino SJY, Gosu V, Hong S, Choi S (2015) Role of computer-aided drug design in modern drug discovery. Arch Pharm Res Springer 38:1686–1701

Mayer AMS, Glaser KB, Cuevas C, Jacobs RS, Kem W, Little RD et al (2010) The odyssey of marine pharmaceuticals: a current pipeline perspective. Trends Pharmacol Sci Elsevier 31(6):255–265

Mitra S, Dash R (2018) Structural dynamics and quantum mechanical aspects of shikonin derivatives as CREBBP bromodomain inhibitors. J Mol Graph Model Elsevier 83:42–52

More-Adate P, Lokhande KB, Shrivastava A, Doiphode S, Nagar S, Singh A et al (2024) Pharmacoinformatics approach for the screening of Kovidra (Bauhinia variegata) phytoconstituents against tumor suppressor protein in triple negative breast cancer. J Biomol Struct Dyn Taylor Francis 42(8):4263–4282

Mujtaba S, He Y, Zeng L, Yan S, Plotnikova O, Sanchez R et al (2004) Structural mechanism of the bromodomain of the coactivator CBP in p53 transcriptional activation. Mol Cell Elsevier 13(2):251–263

O'Boyle NM, Banck M, James CA, Morley C, Vandermeersch T, Hutchison GR (2011) Open Babel: an open chemical toolbox. J Cheminform BioMed Cent 3(1):1–14

Oh K-B, Mar W, Kim S, Kim J-Y, Lee T-H, Kim J-G et al (2006) Antimicrobial activity and cytotoxicity of bis (indole) alkaloids from the sponge Spongosorites Sp. Biol Pharm Bull Pharm Soc Japan 29(3):570–573

Pandey K, Lokhande KB, Swamy KV, Nagar S, Dake M (2021) In silico exploration of phytoconstituents from Phyllanthus emblica and Aegle marmelos as potential therapeutics against SARS-CoV-2 RdRp. Bioinform Biol Insights 15:11779322211027404

Picaud S, Fedorov O, Thanasopoulou A, Leonards K, Jones K, Meier J et al (2015) Generation of a selective small molecule inhibitor of the CBP/p300 bromodomain for leukemia therapy. Cancer Res AACR 75(23):5106–5119

Pon Sathieshkumar P, Nagarajan R (2017) Total synthesis of Metagenetriindole A and Deoxytopsentin. ChemistrySelect. Wiley Online Libr 2(4):1686–1688

Rooney TPC, Filippakopoulos P, Fedorov O, Picaud S, Cortopassi WA, Hay DA et al (2014) A Series of Potent CREBBP Bromodomain

Ligands reveals an Induced-Fit Pocket stabilized by a Cation–π Interaction. Angewandte Chemie Int Ed Wiley Online Libr 53(24):6126–6130

Saeed AFUH, Su J, Ouyang S (2021) Marine-derived drugs: recent advances in cancer therapy and immune signaling, vol 134. Biomedicine & Pharmacotherapy. Elsevier, p 111091

Scott WRP, Hünenberger PH, Tironi IG, Mark AE, Billeter SR, Fennen J et al (1999) The GROMOS biomolecular simulation program package. J Phys Chem ACS Publications 103(19):3596–3607

Shaker B, Ahmad S, Lee J, Jung C, Na D (2021) In silico methods and tools for drug discovery. Comput Biol Med. Elsevier 137:104851

Sharma A, Vora J, Patel D, Sinha S, Jha PC, Shrivastava N (2022) Identification of natural inhibitors against prime targets of SARS-CoV-2 using molecular docking, molecular dynamics simulation and MM-PBSA approaches. J Biomol Struct Dyn Taylor Francis 40(7):3296–3311

Shukla R, Tripathi T (2020) Molecular dynamics simulation of protein and protein–ligand complexes. Computer-aided drug design. Springer, pp 133–161

Singh JK, Dubey S, Srivastava G, Siddiqi MI, Srivastava SK (2023) Neohesperidin and spike RBD interaction in omicron and its subvariants: in silico, structural and simulation studies. Comput Biol Med Elsevier 152:106392

Song X, Xiong Y, Qi X, Tang W, Dai J, Gu Q et al (2018) Molecular targets of active anticancer compounds derived from marine sources. Mar Drugs MDPI 16(5):175

Spiliotopoulos D, Zhu J, Wamhoff E-C, Deerain N, Marchand J-R, Aretz J et al (2017) Virtual screen to NMR (VS2NMR): Discovery of fragment hits for the CBP bromodomain. Bioorg Med Chem Lett Elsevier 27(11):2472–2478

Spriano F, Gaudio E, Tarantelli C, Golino G, Cascione L, Zucca E et al (2018) Targeting both BET and Crebbp/EP300 proteins with the novel dual inhibitor NEO2734 leads to more preclinical antitumor activity in diffuse large b cell lymphomathan with single BET or Crebbp/EP300 inhibitors. Blood Elsevier 132:4174

Studio D (2008) Discovery studio. Accelrys [2.1]

Su JY, Meng YH, Zeng LM, Fu X, Schmitz FJ (1994) Stellettin A, a new triterpenoid pigment from the marine sponge Stelletta tenuis. J Nat Prod ACS Publications 57(10):1450–1451

Tasdemir D, Marshall KM, Mangalindan GC, Concepción GP, Barrows LR, Harper MK et al (2001) Deoxyamphimedine, a new pyridoacridine alkaloid from two tropical Xestospongia sponges. J Org Chem 66(9):3246 [Easton, Pa., etc.] American Chemical Society

Taylor AM, Côté A, Hewitt MC, Pastor R, Leblanc Y, Nasveschuk CG et al (2016) Fragment-based discovery of a selective and cell-active benzodiazepinone CBP/EP300 bromodomain inhibitor (CPI-637). ACS Med Chem Lett ACS Publications 7(5):531–536

Trott O, Olson AJ (2010) AutoDock Vina: improving the speed and accuracy of docking with a new scoring function, efficient optimization, and multithreading. J Comput Chem Wiley Online Libr 31(2):455–461

Unzue A, Xu M, Dong J, Wiedmer L, Spiliotopoulos D, Caflisch A et al (2016) Fragment-based design of selective nanomolar ligands of the CREBBP bromodomain. J Med Chem ACS Publications 59(4):1350–1356

Van De Waterbeemd H, Gifford E (2003) ADMET in silico modelling: towards prediction paradise? Nat Rev Drug Discov. Nat Publishing Group UK Lond 2(3):192–204

van Gils N, Canales TM, Vermue E, Rutten A, Denkers F, van der Deure T et al (2021) The novel oral BET-CBP/p300 dual inhibitor NEO2734 is highly effective in eradicating acute myeloid leukemia blasts and stem/progenitor cells. Hemasphere 5(8):e610

Veríssimo ACS, Pacheco M, Silva AMS, Pinto DCGA (2021) Secondary metabolites from marine sources with potential use as leads for anticancer applications. Molecules MDPI 26(14):4292

Vidler LR, Brown N, Knapp S, Hoelder S (2012) Druggability analysis and structural classification of bromodomain acetyl-lysine binding sites. J Med Chem ACS Publications 55(17):7346–7359

Wang L, Lu D, Wang Y, Xu X, Zhong P, Yang Z (2023) Binding selectivity-dependent molecular mechanism of inhibitors towards CDK2 and CDK6 investigated by multiple short molecular dynamics and free energy landscapes. J Enzyme Inhib Med Chem Taylor Francis 38(1):84–99

Xu M, Unzue A, Dong J, Spiliotopoulos D, Nevado C, Caflisch A (2016) Discovery of CREBBP bromodomain inhibitors by high-throughput docking and hit optimization guided by molecular dynamics. J Med Chem ACS Publications 59(4):1340–1349

Xu H, Luo G, Wu T, Hu J, Wang C, Wu X et al (2022) Structural insights revealed by the cocrystal structure of CCS1477 in complex with CBP bromodomain. Biochem Biophys Res Commun Elsevier 623:17–22